Non-lethal imaging and modeling approaches for estimating dry mass in aquatic larvae

Short Title: Estimating dry mass in aquatic larvae

Authors: Daniela Granados Frias[1], Najva Akbari[1], Lauren A. O'Connell[1], Bryan H. Juarez[1,2,*]

[1]Department of Biology, Stanford University, Stanford, CA 94305, USA

[2]Earth System Science Department, Stanford University, Stanford, CA 94305, USA

***Corresponding Author Email:** bryanhjuarez@gmail.com

ORCIDs: O'Connell: 0000-0002-2706-4077; Juarez: 0000-0002-5474-596X

Author contributions: DGF: Data Curation, Funding Acquisition, Investigation, Methodology, Resources, Software, Validation, Visualization, Writing – Original Draft Preparation, Writing – Review & Editing, NA: Funding Acquisition, Methodology, Resources, Validation, Visualization, Writing – Review & Editing, LAO: Funding Acquisition, Resources, Supervision, Visualization, Writing – Review & Editing, BHJ: Conceptualization, Data Curation, Formal Analysis, Investigation, Methodology, Project Administration, Resources, Software, Supervision, Validation, Visualization, Writing – Original Draft Presentation, Writing – Review & Editing.

Key Words: regression, deep learning, neural network, random forest, adaptive lasso, Fiji, ImageJ, ontogeny

Word Count: 5,653

Resumen

La masa corporal es crucial para escalar y comparar las tasas fisiológicas. Por ejemplo, la masa corporal seca es importante para determinar la tasa metabólica de un organismo, ya que excluye el peso del agua metabólicamente inactiva. Obtener medidas repetidas de la masa corporal a lo largo de la vida de un individuo es trivial. En cambio, normalmente solo podemos obtener una única estimación de la masa corporal seca por individuo, ya que los métodos clásicos requieren la eutanasia final seguida del secado. Presentamos técnicas de imagen y modelado para estimar la masa corporal seca individual en renacuajos de rana Africana de uñas (*Xenopus laevis*), permitiendo el muestreo repetido de los mismos individuos. Aplicamos principios alométricos y comprobamos si la anatomía externa proporcionaría estimaciones fiables de la masa corporal seca. En concreto, describimos un procedimiento para integrar renacuajos en medios de agarosa para obtener datos morfológicos en 3D y, a continuación, evaluamos las predicciones de masa seca entre nueve modelos de máxima probabilidad y aprendizaje automático con validación cruzada. El modelo con mejor rendimiento y flexibilidad es un modelo alométrico que utiliza estimaciones del volumen corporal para predecir la masa corporal seca (r^2 de validación = 0,75). Sin embargo, otros modelos basados únicamente en la masa corporal húmeda o diseñados para reducir el número de variables de entrada necesarias también pueden ser logísticamente viables. Analizamos las ventajas, desventajas y futuras direcciones de los nueve modelos y ofrecemos consejos prácticos para la recopilación y el análisis de datos. Esta investigación sienta una base sólida para la investigación continua sobre la importancia biológica de la masa corporal seca, en particular en el contexto del crecimiento y la ecología fisiológica. El desarrollo futuro de enfoques similares es crucial para comprender la importancia de los índices de masa corporal para la estandarización y comparación de las tasas fisiológicas en plantas y animales.

Abstract

Body mass is crucial for scaling and comparing physiological rates. For example, dry body mass is important in determining an organism's metabolic rate since it excludes metabolically inactive water weight. Obtaining repeated measurements of body mass throughout an individual's lifetime is trivial. In contrast, we are normally able to obtain only a single estimate of dry body mass per individual since classical methods require end-point euthanasia followed by drying. We present imaging and modeling techniques for estimating individual dry body mass in African clawed frog (*Xenopus laevis*) tadpoles, which allows repeated sampling of the same individuals. We applied allometric principles and tested whether external anatomy would yield reliable estimates of dry body mass. Specifically, we describe a procedure to embed tadpoles in agarose media for obtaining morphological data in 3-D and then we evaluate dry mass predictions among nine cross-validated maximum likelihood and machine learning models. The best performing and flexible model is an allometric model that uses estimates of body volume to predict dry body mass (validation r^2 = 0.75). However, other models based only on wet body mass or meant to reduce the number of necessary input variables may also be logistically tractable. We discuss the pros, cons, and future directions of all nine models and give practical advice for users on data collection and analysis. This research develops a strong foundation for continued research on the biological importance of dry body mass, particularly in the context of growth and physiological ecology. Future development of similar approaches is crucial for understanding the importance of body mass indices for standardization and comparison of physiological rates in plants and animals.

Introduction

Body mass is a key feature used to understand processes in form, function, ecology, and evolution. For example, body size is central in studies of organismal growth and development [1–3], physiology [4–6], movement and distribution [7–9], ecogeographical gradients [10–12], and even survival [13]. In the fields of physiological ecology or evolutionary ecology [14], body mass is necessary for understanding the mechanisms that drive the empirical pattern of metabolic scaling [5,15,16] and comparing physiological rates among cells, tissues, individuals, or species of different sizes [5,17–22]. Researchers have quantified mass in many ways when performing comparisons of physiological rates.

Common body mass indices include wet (live), dry, or fat-free (lean) mass and they are used for a variety of purposes. For example, the different body mass indices include wet mass [23–29], dry mass [23,25,27,29–31], lean mass [23,24,32], dry lean mass [23], or combinations thereof [23,25–27,29,33]. The choice of mass index can depend on the logistics of data collection in the field or lab, affordability, or model assumptions related to correlations among the different mass indices and selected physiological rates. For example, dry body mass is used as an indicator of metabolic rate since it factors out the non-metabolizing mass of water in the body. Previous work required transformations among body mass indices, such as among dry and wet mass [34,35], but these types of tools are not widely available for many taxa. Furthermore, many of the latter indices are typically only obtainable once following euthanasia. While available tools let us evaluate correlations between wet body mass and physiological rates through time [36–38], the same does not apply to other mass indices. The latter is a barrier in physiological research since it limits our ability to investigate relationships between body mass indices and physiological rates through time, such as across the seasons, development, or throughout the lifespan. Instead, researchers depend on relating repeated measurements of physiological rate through time with a single estimate of body mass obtained at or near the experimental endpoint [23,39,40] or by comparing population means between discretely modeled time points like seasons [25,29]. The goal of this study is to develop a predictive model for obtaining repeated

estimates of dry body mass on the same individuals without the need for euthanasia, thus reducing the number of euthanized animals needed in future experiments.

Here, we describe approaches for estimating dry body mass using morphometrics. Body mass is the net result of an animal's metabolic needs and energy consumption, in other words, body mass is the product of growth [5,15,41]. Since growth may also be expressed not by an organism’s mass, but by an organism’s volume, we can express growth in terms of changes in volume [42–44]. Next, just as whole-animal measurements of mass-specific metabolic rates average together all tissue types [34], one approach for estimating body mass from body volumes is to average together the density of all tissue types such that the relationship between the logarithms of mass and volume follows an allometric scaling (power) law [3,45,46]. In a simple example using a sphere of uniform density, volume is directly proportional to mass. The surface area and length (radius) of the sphere are also proportional to mass, but estimation or measurement errors can make either measurement a suboptimal predictor of the mass of the sphere. To obtain reliable estimates of dry body mass, we can empirically estimate a linear transformation between body volume (or areas and lengths) and body mass after drying.

Despite the importance of body mass indices other than wet (live) body mass, few researchers have attempted to develop surrogates for dry or lean body mass in vertebrates. Most research in this area comes from plant biology where the dry body mass of leaves was estimated from the product of surface area and the average optical path difference of the cells in water [47]. The method was validated using model spheres and performed as predicted from theory. Others have used data on tree height, diameter, and age with density and volume models to estimate stem dry mass [48]. In animals, both length [49,50] and other body measurements [51] are significantly correlated to dry body mass in terrestrial and aquatic invertebrates. Live body mass and head width have also been used as predictors of dry body mass in insects including both dried specimens and those contained in dehydrating preservatives [52]. In vertebrates, similar studies have focused on quantifying water loss following preservation as a function of initial wet body mass [53–56]. Other studies in adult amphibians have used allometric models to estimate animal or tissue volumes using

linear measurements [57–59]. While wet body mass is an indicator of water loss during preservation, we still lack a general understanding of how morphology, animal or tissue volumes, and dry body mass are linked in vertebrate animals. Overall, morphological and empirical approaches are promising in developing predictive models of dry mass or dehydrating processes.

Amphibian larvae are a great system for learning how anatomy varies with dry body mass. Specifically, anuran (frog and toad) tadpoles are easy to work with and are commercially available. For example, clawed frog (*Xenopus*) larvae are easily obtainable, the husbandry is simple [60,61], and the small size of tadpoles makes them amenable to studies of functional morphology and metabolic rates alike. The larvae of many frogs, including *Xenopus*, and toads are also partly translucent, allowing for easy measurement of a variety of traits. The small body size of tadpoles and their permeable skin makes them dry quickly, relative to larger vertebrates. Looking forward, amphibian larvae have varied diets and exhibit plastic morphologies, developmental rates, and reproductive or social behaviors, making them a target for applied research [62–68]. This study opens the doors for understanding how abiotic and biotic factors impact physiology, growth, and development through an organism's life, independently of non-metabolizing water content in the body.

The purpose of this study is to design new tools for obtaining repeated measures of dry body mass from the same individuals without harming live animals. Additionally, we seek to estimate the relationship between wet and dry body mass which is important in transforming between different body mass indices. Following allometric principles, we hypothesize that morphology is a strong indicator of dry body mass. We predict that body volume is a significant predictor of dry body mass and that body volume is the best predictor of dry body mass relative to surface areas and lengths, possibly due to the limitations of using predictors of lower dimensions when predicting dry body mass. In this study, we demonstrate how we may reliably estimate dry body mass using several alternative models and these models are suitable for obtaining dry body mass through ontogeny.

Methods and Materials

Animals and housing

This study was approved by the Stanford University under the Administrative Panel on Laboratory Animal Care (APLAC, Protocol #33097). *Xenopus laevis* tadpoles of Gosner stages 44–54 (N=61; Xenopus 1, Corp (Dexter, Michigan, USA) were placed into aquaria (18.09 cm L x 11.13 cm W x 13.34 cm H). The tank included 0.1X Marc's modified Ringer's solution (MMR) to avoid osmotic stress [69], shelter made of PVC pipe, and an air pump with a bubbling stone to aerate the water tank. Tanks were maintained at 25C and 50% water changes (0.1X MMR) were performed every 2 days and as needed. Tadpoles were fed crushed tadpole food pellets (Josh's Frogs, Owosso, Michigan, USA) three times per week. Animals were isolated for 24 hours without food prior to further experimentation to allow time for defecation and to avoid confounding our estimates of wet and dry body mass with food mass.

Imaging and data collection

Tadpole embedding, imaging, and measurement methods are available in a step-by-step guide at protocols.io: dx.doi.org/10.17504/protocols.io.rm7vzk1wrvx1/v1 [70]. Each tadpole was anesthetized in a container with 10 mL of 0.03% buffered MS-222 for roughly 1 min. We lightly brushed the tadpole's body with a paint brush to confirm successful anesthesia. Next, we filled a chambered coverglass (5 cm L x 2 cm W x 1 cm H; Thermo Scientific, Waltham, Massachusetts, USA) halfway with 1.5% melted agarose at 42 ℃. We placed the tadpole into this chamber and positioned its body parallel to the length of the coverglass, but closer to one corner of the coverglass to improve the quality of the photographs and measurements. Placing the tadpole medially and parallel to the length of the coverglass resulted in poor quality photographs and measurement accuracy during preliminary trials. We then confirmed optimal body positioning and added 2-3 drops of MS-222 with a plastic transfer pipette to ensure anesthesia throughout the entire imaging process, and then filled the chambered coverglass containing the tadpole with melted agarose. *Ad hoc* addition of MS-222 was necessary (e.g., if the tadpole twitched) to guarantee the efficacy of the procedure for all tadpoles.

Embedding tadpoles in the chambered coverglass allowed imaging of the whole tadpole from all three dimensions (dorsal, lateral, and frontal). Images were taken using a Leica Si9 microscope at a magnification of 0.6x and 1x. The pictures were taken using the default settings in the LAS EZ v. 3.4.0 (Leica Microsystems, Wetzlar, Germany). We included 1 mm grid paper placed in the same horizontal plane as the tadpole in every image to convert pixels to real distances. After imaging, we removed the tadpoles from the agarose media by gently breaking apart the agarose using a paint brush and then placed them into conditioned (isotonic) DI water to remove any agarose clinging onto the body. Once clean, we transferred the tadpoles into a petri dish to remove excess water and obtained the wet mass on an analytical scale (Model PMF523/E, Fisher Scientific, Pittsburgh, United States).

We euthanized the tadpoles by applying 20% benzocaine gel to the body and confirming the animal was unresponsive prior to flash freezing in liquid nitrogen. Briefly, a small petri dish was placed in a container filled with liquid nitrogen until equilibrium was reached. The petri dish was then moved to an insulated container and filled with liquid nitrogen. Then, we placed the tadpole into the liquid nitrogen and covered the petri dish with a lid. The insulated container was filled with liquid nitrogen until the petri dish was halfway immersed. The container was then covered with a lid to minimize heat transfer. We weighed the tadpoles on a pre-weighed glass slide 15 minutes after flash freezing to guarantee euthanasia. Next, we placed the glass slide with the tadpole in a separate petri dish and moved it to a drying oven set at 37°C and left to dry for up to 72 hours. The dry mass was obtained by subtracting the weight of the glass slide from the final weight of the dried tadpole on the glass slide.

We obtained 15 measurements from each tadpole image using Fiji v. 1.54f [71]. These 15 measurements (see Fig. 1, Fig. S1) included (1) the dorsal length, width, and area for the body and the tail, (2) the lateral body height, tail length and height, and the body, tail, tail muscle, and limb bud areas, and (3) the frontal body width and area. We also obtained 10 additional variables, including tail muscle area, and tail and body volume estimated in different ways. Including the animal's wet and dry mass, we obtained 27 (15+10+2) measurements from each tadpole (Table 1).

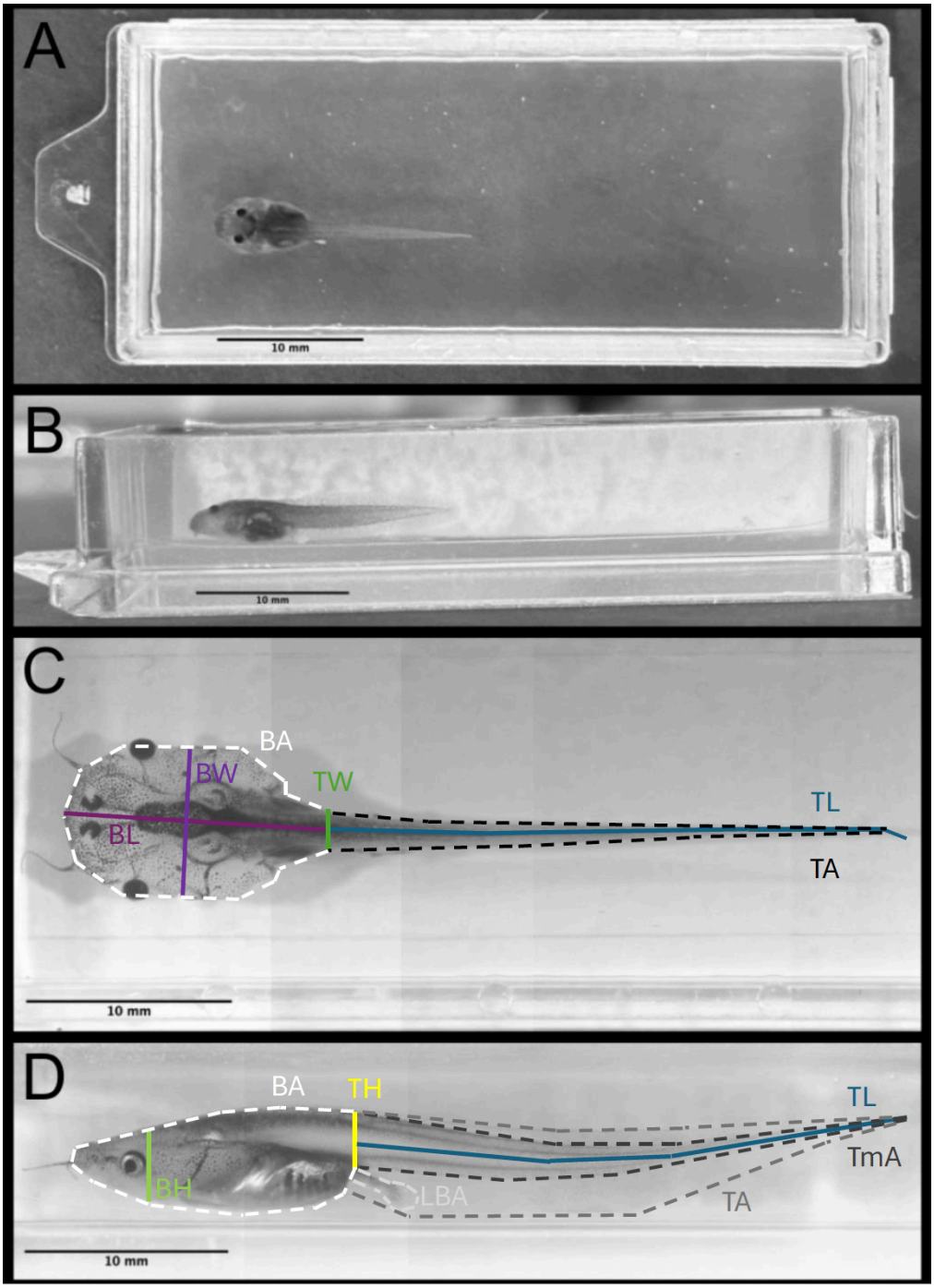

Figure 1. Tadpoles embedded in agarose media and anatomical traits measured. A. Image showing agarose-embedded tadpole in chambered coverglass from dorsal view. B. Image showing agarose-embedded tadpole in chambered coverglass from lateral view. C. Dorsal measurements obtained in this study (see Table 1). D. Lateral measurements obtained in this study (see Table 1). BL is body length, BW is body width, BL is body height, BA is body area, TL is tail length, TW is tail width, TH is tail height, TA is tail area, TmA is tail muscle area, and LBA is limb bud area. Images C, D are composite images obtained by stitching individual images (see Methods and Materials).

Table 1. Initial input variables used in all models. M is model (see Data analysis in Methods). View is the 3-dimensional origin of each trait. NA is not available, L is lateral, D is dorsal, F is frontal, and Composite is traits obtained from two views. T is tail, Tm is tail muscle, B is body, A is area, L is length, W is width, and H is height. 1 and 2 indicate traits included in the initial and final fits for each model (M1–8), respectively.

View	Units	Trait	Description	M1	M2	M3	M4	M5	M6–8
NA	g	wet mass		1, 2					1, 2
Dorsal	mm	body length	snout-vent		1				1, 2
	mm	body width	postorbital width		1				1, 2
	mm	tail length	vent to end of tail		1				1, 2
	mm	tail width	width at vent		1, 2				1, 2
	mm^2	body area				1			1, 2
	mm^2	tail area				1, 2			1, 2
Lateral	mm	body height	postorbital height		1, 2				1, 2
	mm	tail length			1, 2				1, 2
	mm	tail height	height at vent		1, 2				1, 2
	mm^2	body area				1			1, 2
	mm^2	tail area				1			1, 2
	mm^2	tail muscle area				1			1, 2
	mm^2	fin area	LTA-LTmA			1, 2			1, 2
	mm^2	limb bud area			1, 2	1, 2			1, 2
Frontal	mm	body width	eye to eye		1, 2				1, 2
	mm^2	body area				1, 2			1, 2
Composite	mm^3	body volume 1	LBA*DBW				1		1, 2
	mm^3	body volume 2	LBA*FBW				1		1, 2
	mm^3	body volume 3	LBH*DBA				1, 2		1, 2
	mm^3	body volume 4	DBL*FBA				1		1, 2
	mm^3	tail volume 1	LTA*DTW				1		1, 2
	mm^3	tail volume 2	LTH*DTA				1		1, 2
	mm^3	tail muscle volume	LTmA*DTW				1, 2		1, 2
	mm^3	body volume 5	LBH*DBL*DBW					1, 2	1, 2
	mm^3	tail volume 3	LTH*DTL*DTW					1, 2	1, 2

Data analysis

We compared the performance of eight models to test our predictions that morphology, namely body volumes, are reliable estimators of dry body mass. The eight models include those of wet body mass (model 1), length measurements (model 2), surface areas (model 3), volumes (models 4–5) and all data (models 6–9). The first five models were ordinary least squares (OLS) regression models based on maximum likelihood. The final four were machine learning models including one random forest, two adaptive lasso, and one neural network. The first lasso model sparsely optimized the mean square error while the second gave the sparsest model within one standard error of the minimum loss (mean square error). We included machine learning models since each has beneficial properties that may outperform likelihood-based models. For example, random forest models allow for the modeling of potential non-linearities, the adaptive lasso optimizes prediction ability while reducing the number of necessary input variables and exhibits the oracle property [72], neural networks can model all possible interactions in a dataset, and all can perform automatic feature selection (taking multicollinearity into account). We used variance inflation factors (VIF) and a cutoff of VIF = 10 to remove collinear terms from each likelihood model [73]. For example, we obtained estimates of body width from both dorsal and lateral views but either may serve as an optimal predictor of dry mass. We show the initial and final variables for each model in Table 1. We natural log-transformed all data except limb bud area which we square root transformed since some tadpoles did not have limb buds. Finally, we evaluated prediction ability in each model after confirming that each model exhibited appropriate model diagnostics.

We used repeated K-fold cross-validation to evaluate model performance as determined primarily by the mean square error and its standard deviation. We also measured the mean absolute error, r^2, and their standard deviations. Specifically, we used 200 repeats of 5-fold cross-validation to guarantee each randomly sampled validation set contained at least 10 samples (N = 61 samples / 5 folds = 12.2 samples per validation set) and to estimate error for each prediction metric using at least 1,000 (200 x 5) validation sets. We implemented this procedure for models 1–6 using the caret package v. 6.0-94 in R version 4.4.1 [74,75]. To obtain comparable metrics for the

adaptive lasso, we back-calculated the population mean and standard deviations for all performance metrics across 200 samples of (non-repeated) 5-fold cross-validation using the R package glmnet 4.1-8 [76,77]. We were not able to obtain estimates for the r^2 of the adaptive lasso since this is not currently implemented in glmnet 4.1-8. Next, we describe how we fitted the neural network model and obtained its performance metrics.

We implemented a feed-forward neural network using keras3 v. 1.2.0 and tensorflow v. 2.16.0 in R [78,79]. Prior to fitting the model, we split the data into 60-20-20% training, validation, and testing sets to guarantee the model validation and testing steps were performed on at least 12 samples and the model was trained using at least 30 (N = 36) samples. In general, neural networks use the training set to sample network parameters, the validation set to tune hyperparameters and evaluate model performance after each gradient update, and the testing set to give an unbiased estimate of out-of-sample model performance for unseen data (as in standard cross-validation). We selected hyperparameters by determining the hyperparameter combination that resulted in the lowest validation error (mean square error). Here, we define validation error as the median of 3 replicate model fits for each hyperparameter combination. This is necessary to reduce sampling error since fitting neural networks includes a stochastic component that affects model performance. The hyperparameters we varied included the number of neural layers from 0 to 25 (by one) and the number of neurons per layer from 200 to 2,500 (by 100), each using a learning rate of 0.001 across 200 epochs. We selected this arbitrarily broad range after determining the standard suggestions of 1–3 layers and neurons per layer of 0.5X, 1X, and 2X the sample size did not yield usable results, but we still included these in the hyperparameter search [80–82]. We also applied a stop rule to end sampling if the validation error (mean square error) did not decrease after 50 epochs to protect against oversampling local minima across the search space and decrease computation time. We obtained the final out-of-sample performance metrics (mean square error, mean absolute error, and r^2) using the testing set. All sampled networks contained a normalizing layer (to improve model quality and reduce computation time), used Rectified Linear Unit (ReLU) activation for signal propagation (to avoid vanishing gradients), and an Adam optimizer for automatic tuning of the learning rate [83,84].

Results

Overall, we found that most models exhibited statistically similar prediction ability with notable differences in the AICc of likelihood models and in the validation or testing mean square error of each model (Fig. 2; Table 2). We provide equations and relevant statistics for each model in Tables 3–9. Since the random forest model (6) and neural network model (8) have thousands and hundreds of thousands of parameters, respectively, we also provide code to fit all models in this study (To be updated after acceptance: dryad.org/; github.com/). Tadpoles were 22.48–46.04 mm (mean = 33.67, std. dev. = 5.50) in total length, exhibited wet body masses of 4.745–4.982 g (mean = 4.834, std. dev. = 0.062), and had dry body masses of 0.002–0.017 (mean = 0.008, std. dev. = 0.004). We found all tadpoles dried completely within 48 hours. We describe each model below.

The likelihood models (1–5) exhibited statistically similar validation metrics (Fig. 2), with Model 5 standing out as the single best likelihood model according to AICc (Table 2). The wet body mass model (1) yielded the predictions with the lowest accuracy (highest validation error). The mean absolute error of the natural log of wet body mass was 0.3050 and yields a mean percentage error of 35.66% = $(e^{0.3050} - 1)\ x\ 100\%$ (Fig. 3). Despite this, wet body mass is a significant predictor of dry body mass in the measured tadpoles (Table S1; F = 89.342, p < 0.001). The lengths model (2) ranked among the worst models and exhibited a mean percentage error of 29.19%. The dorsal tail width, lateral body height, and lateral tail height were all significant predictors of dry body mass (Table S2; F = 13.564–122.775, $p \leqq 0.001$). The surface area model (3) was among the worst performing models with a mean percentage error of 30.51%. Model 3 had two significant predictors including lateral fin area (F = 8.030, p = 0.006) and dorsal tail area (F = 118.955, p < 0.001). The volumes model (4), whose volumes were estimated from areas and lengths, ranked among the best models (Table 2). Model 4 exhibited a mean percentage error of 27.02%. Its significant predictors included body volume as estimated from the product of lateral body height and dorsal body area (F = 155.779, p <0.001) and tail muscle volume which we obtained as the product of lateral tail muscle area and dorsal tail width (F = 8.237, p =0.006) . The last model based on likelihood, model 5, ranked highest among the surveyed likelihood models

and had a mean percentage error of 27.00% (Fig. 3). Its predictors included body volume (F = 161.939, p < 0.001) estimated as the product of dorsal body length, dorsal body width, and lateral body height , and tail volume (F = 10.111, p = 0.002) obtained as the product of dorsal tail length, dorsal tail width, and lateral tail height. Next, we describe the performance of the machine learning models (6–8) included in this study.

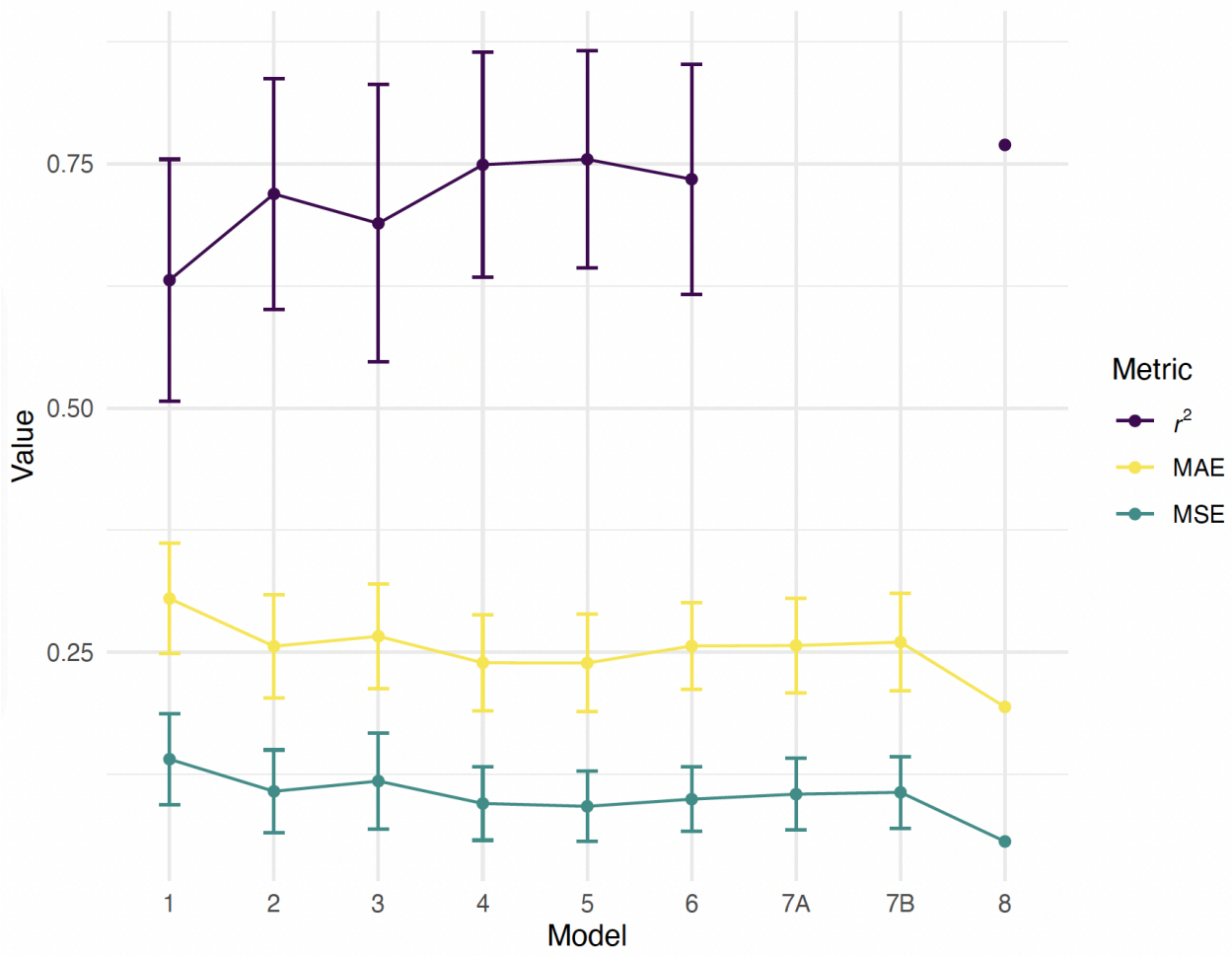

Figure 2. Plot of performance metrics for surveyed models. Models are as in Table 1 and the main text. Models 1–6 are likelihood models and models 6–8 are machine learning models. MAE is the mean absolute error and MSE is the mean square error. Error bars indicate ∓ 1 standard deviation of the mean. r^2 is not implemented for Model 7. Model 8 lacks error bars because metrics are based on a single testing set of N = 12. The theoretical best model has a high r^2 and low errors (MAE or MSE).

Table 2. Performance metrics for surveyed models. Rank is the model rank based on MSE and shown only for validation metrics obtained using repeated K-fold cross validation. # Var is the number of final predictor variables. AICc is the Akaike Information Criterion corrected for small sample size for likelihood models. MSE is the mean square error. MAE is the mean absolute error. r^2 is the coefficient of determination. SD is the standard deviation. r^2 is not implemented for Model 7. Model 8 lacks standard deviation estimates because metrics are based on a single testing set of N = 12. The theoretical best model has a high r^2, low errors (MAE or MSE), and a low AICc.

Model (Rank)	# Var	AICc	MSE	MAE	r^2	MSE SD	MAE SD	r^2 SD
1 (8)	1	56.4515	0.1405	0.3050	0.6310	0.0469	0.0566	0.1237
2 (6)	6	38.1121	0.1076	0.2561	0.7192	0.0424	0.0530	0.1182
3 (7)	5	46.4331	0.1181	0.2663	0.6891	0.0494	0.0536	0.1420
4 (2)	2	33.1050	0.0952	0.2392	0.7491	0.0376	0.0491	0.1152
5 (1)	2	30.9366	0.0922	0.2390	0.7546	0.0358	0.0498	0.1110
6 (3)	26	-	0.0996	0.2564	0.7343	0.0331	0.0447	0.1179
7A (4)	6	-	0.1047	0.2568	NA	0.0368	0.0482	NA
7B (5)	5	-	0.1066	0.2603	NA	0.0368	0.0498	NA
8	26	-	0.0563	0.1940	0.7694	NA	NA	NA

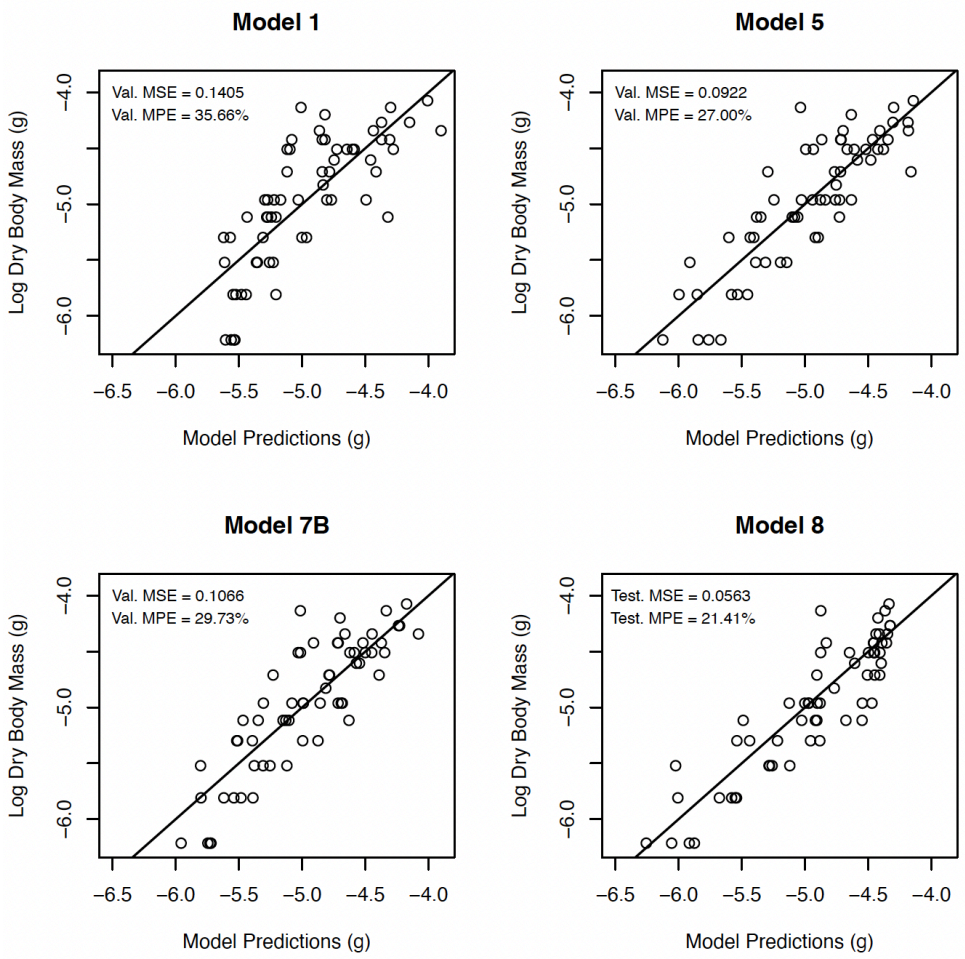

Figure 3. Actual versus predicted plots comparing the wet body mass model (1) to the best likelihood (5), machine learning (7B), and neural network models (8). Each point is an individual tadpole. Val. MSE is the validation mean square error and Val. MPE is the validation mean percentage error. Test. MSE and Test. MPE are the mean square error and mean percentage error for the testing set of Model 8. The solid line is the 1:1 line. The theoretical best model has low errors (MSE, MPE).

As a whole, the machine learning models provide flexible and similar alternatives to likelihood models (Fig. 2; Table 2). After automatic tuning of the number of variables per split (m = 2), the random forest model (6) yielded a mean percentage error of 29.23%. Estimates of variable importance, or the average decrease in mean square error after splitting on each variable, are in Table S6. Briefly, lateral body area was the most important variable (importance = 1.231) and the lateral limb bud area was the least important (importance = 0.276). The adaptive lasso model (7) yielded a variety of sparse solutions, where some regression parameters are set to 0, depending on the

regularization parameter λ. Two solutions include the optimal sparse prediction model (minimum λ; Model 7A) and the sparsest model within one standard error of the minimum λ (Model 7B). The mean percentage errors for Model 7A and B were 29.28% and 29.73% (Fig. 3), respectively. Table S7 shows the selected variables and coefficient estimates for Models 7A and B. Model 7A selected the wet body mass, dorsal body length, dorsal tail width, lateral body height, and lateral tail height as predictors. Model 7B selected the same variable set as 7A, but excluded dorsal tail width. Finally, the hyperparameter search for the neural network model (8) showed 11 layers and 1900 neurons per layer gave the lowest validation error among surveyed network structures (Fig. 4). The hyperparameter search results are found in the Supplementary Material (Table S8). We estimated network parameters using the latter hyperparameters and found a mean square error of 0.0563 (Fig. 2; Table 2) and mean percentage error of 21.41% for the testing set (Fig. 3).

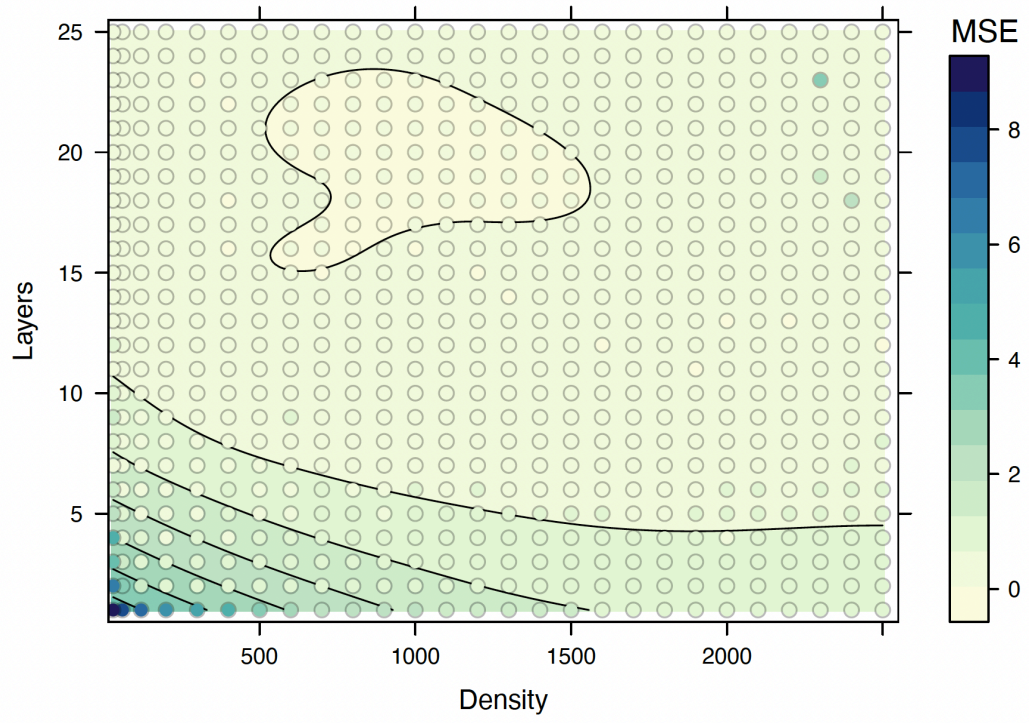

Figure 4. Level plot of hyperparameter search results for neural network (Model 8). Layers is the number of neural layers, density is the number of neurons per layer, and MSE is the (validation) mean square error. Contour lines generally correspond to the discrete differences in MSE shown in the legend. The network with the lowest validation error had 11 layers and 1900 neurons.

Discussion

Here we present a new method that allow future users to estimate the dry body mass of a vertebrate more than once through its lifetime and without lethality. In other words, researchers need only take photographs, measure tadpoles, and apply the regression equations of their choice (Models 1–8) to estimate dry body mass continuously through an animal's life. Specifically, the results support our predictions that body volumes are good predictors of dry body mass. However, we did not predict surface areas would perform worse than lengths in predicting dry body mass. This is likely due to the fact that using surface areas as a predictor of dry body mass benefits neither from direct estimation of volumes nor benefits from using many independent predictors (lengths), leading to a relatively inaccurate geometric model connecting spatial dimensions with dry body mass. We also found wet body mass alone is a relatively poorer indicator of dry body mass in tadpoles when compared to morphology. Additionally, machine learning models that combine morphological information with wet body mass provide some logistical benefits when estimating dry body mass which come with a small cost to prediction accuracy. While the neural network showed viable prediction metrics which were similar to other models, practical and conceptual issues may limit its use in future studies. Below, we discuss our findings in detail, offer some best practices for users of these methods, and discuss some future directions of this research, particularly within the field of physiological ecology.

We found several viable modeling alternatives for predicting dry mass. Most models exhibited similar variances with small differences in mean validation metrics (Table 2). AICc showed a better fit for the volumes based model (5) compared to all other likelihood models, but some of these models may still be of practical use to many readers. For example, the wet body mass model (1) underperformed relative to model 5 (ΔAICc = 25.51; ΔMSE = 0.0483). Despite this, wet body mass was still a significant predictor of dry body mass (Table S1), it is a quick measurement to obtain, and this approach may be suitable for many study designs if users are willing to accept an increase in the mean percentage error of 8.66% relative to model 5. However, we have found that removing (e.g., blotting) surface water from tadpole bodies is challenging and risks injuring the tadpole. Models 2–4 provide intermediate and viable alternatives for

obtaining estimates of dry body mass and only require users to obtain four to six independent measurements. To obtain accurate estimates of dry body mass using likelihood models, we recommend using Model 5. The latter requires estimating the body and tail volume using six measurements that include: the lateral body height, dorsal body length, dorsal body width, lateral tail height, dorsal tail length, and the dorsal tail width. Below, we describe the surveyed machine learning models which may provide useful alternatives to Models 1–5.

The adaptive lasso should be used with caution but can provide logistical and/or quantitative advantages over Models 1–5. The adaptive lasso features variable selection through regularization, a greater rate of convergence relative to the regular lasso, and the oracle property: with enough data, the adaptive lasso can select the true model [24,72]. However, Models 7A and 7B come with the notable drawback that they require a bias-variance trade-off (proportional to λ) to give optimal predictions. This means that while Model 7 exhibited good validation metrics, it will necessarily output slightly biased estimates of dry body mass to optimize prediction accuracy. Therefore, Model 7 is appropriate for determining the magnitude of group effects and covariances but is not appropriate for accurately estimating or interpreting the dry body mass of individual tadpoles (without bias). With these considerations in mind, Model 7B provides the tractable benefit of requiring only four easy-to-measure traits to nearly reach the prediction accuracies of the most accurate models. The four traits required by Model 7B include wet body mass, dorsal body length, lateral body height, and lateral tail height (Table 9). As seen above, machine learning models can provide many advantages, given that we understand the properties of the implemented model.

The neural network model (8) exhibited good quantitative performance, but it may not be ideal for many situations and comes with many drawbacks. First, we do not have an ideal way of performing model comparisons among neural networks and other model classes. While Model 8 had the lowest mean square error in Table 2, its validation metrics are not comparable to Models 1–7. This is because the validation metrics are based on a single testing set and not cross-validation. While methods such as stratified K-fold cross validation [85] are available for neural networks, this would still require performing a new hyperparameter search for each testing set of interest and

doing this N = 1000 times would be extremely time intensive and computationally expensive. An alternative that would enable direct comparisons to other models would be to define one or many testing sets for all models. However, this comes at the great expense of reducing the sample size of the testing and validation sets for other models. The latter would increase prediction error for models 1–7 and limit estimates of generalizability. A second drawback to using Model 8 for predicting dry mass is that it exhibits the undesirable behavior of predicting the same value for some of the largest tadpoles and this can be seen as a vertical ridge in Fig. 3. This can create major statistical issues for many types of downstream analyses due to the introduction of biases which artificially generate sample homogeneity. Moreover, the latter may result in difficulties meeting the residual homoscedasticity assumptions of linear models. Third, the neural network requires all of the variables in Table 1 to make predictions so users must weigh the time it takes to obtain all measurements against the quality and reliability of the predictions. Fourth, it is very difficult to learn why neural networks exhibit particular behaviors and a deeper understanding of how neural networks make predictions is needed before we are able to use them to predict dry body mass. While obtaining estimates of dry body mass without sacrificing the focal animals can present challenges, next we offer some practical advice for obtaining the morphological data and analyzing the resulting predictions.

There are many practical solutions for flexibly implementing and advancing the models being proposed here. For example, in this study we used agarose media to embed tadpoles in chambered coverglasses but a viable alternative is taking morphological measurements using optical micrometers and measuring tadpoles in chilled water to minimize movement but allow respiration and minimize stress. If users wish to implement end-point euthanasia, measurements may also be taken using photogrammetry [86,87]. In fact, photogrammetry may allow for more accurate estimation of body volume. Future improvements to our models include increasing the sample sizes to allow for larger training, validation, and testing sets. New pseudosamples may also be generated by introducing random noise to the raw data, using growth models to simulate data of intermediate growth stages, or using parametric bootstrapping to draw pseudo samples from a multivariate normal

distribution [88,89]. While each neural network (Fig. 4, Table S8) took 10 seconds to 10 minutes to complete, analyses might be sped up by co-optimizing the learning rate and the optimizer or by limiting the number of input variables. Robust linear models [90,91] might offer solutions for potential heteroscedasticity issues with predictions made from Model 8. We also encourage empirically validating predictions or even comparing predictions among Models 1–8 to determine whether the data qualities suit the needs of downstream analyses. Furthermore, in downstream analyses where dry body mass is used as an independent variable, users may set weights or use measurement error models [92,93] where the weights or errors are proportional to the mean absolute error (log scale) or the mean percentage error (raw scale) reported for each model. For instance, a mean percentage error of 27% (Model 5) applied to the smallest and largest tadpoles in this study gives dry mass errors of ∓ 0.00054 and 0.005g for each, respectively. Other future directions include improving our knowledge of tissue densities and we discuss these next.

Detailed knowledge of tissue densities and how they change over time would greatly improve predictions of dry body mass. Our approach in this study was to assume constant tissue density throughout the body but we relaxed this assumption by modeling some body parts independently of each other. However, the body is made of tissues of varying densities including muscle, cartilage, bone and fat. Knowledge of tissue densities and tissue proportions within body regions would allow us to distinguish the effects of density and dehydration which are inseparable when modeling dry body mass as a simple natural log-linear function of body volumes. Interestingly, the adaptive lasso model (7) included both wet body mass and morphology as predictors, suggesting at least some separation of the effects of density and dehydration. Future research using micro-CT or similar methods might allow us to estimate the volumes of various tissues with distinct densities. However, the density of distinct body regions may vary among individuals or fluctuate as an animal grows and this has presented challenges when modeling dry mass in plants [42]. In amphibians, the skull, limbs, and pelvic region undergo substantial modifications of cartilage and bone through development and particularly during metamorphosis into terrestrial adults [64]. The latter might create non-linearities and interactions in the data space, particularly with the emergence of

adult traits during development. Additionally, the vertebral column in tadpoles may be a great estimator of overall body size or dry body mass in tadpoles and this prediction matches our observation that dorsal tail width was an important predictor of dry body mass found in all models. Specifically, vertebral anatomy is a significant indicator of body size and differences in vertebral anatomy are related to differences in swimming behaviors in other aquatic vertebrates [94–96]. In summary, understanding the density of structures throughout the body and how they change through time is an important area of future research.

The application and future directions of this research should help to advance our understanding of biological processes. We recognize three key areas including identifying the sources of natural variation, the mechanisms underlying growth, and the mechanisms linking populations with macroecological and macroevolutionary patterns. In the context of physiological ecology, learning how body mass channels physiological rates is a question of rich history and open inquiry, with metabolic rates perhaps among the most studied type of physiological rate across taxa [5,15,16,19,34,97,98]. We are still learning how rates might scale up to whole organisms and empirical research often struggles with high degrees of intraspecific variability [16,31,34,99]. Understanding how mass indices, including dry mass, vary within and among tissue types, individuals, and species is necessary for deeper knowledge of physiological rates and recently developed methods allow the integration of intraspecific and interspecific data in a phylogenetic context [100]. In addition, the integration of intraspecific and interspecific data in combination with different body mass indices seems crucial in elucidating the mechanisms underlying metabolic scaling: each body mass index makes different assumptions about how body size and different tissues relate to metabolism through mass, density, and metabolic activity. For example, use of dry body mass in such models measures body size independently of water which does not metabolize. Furthermore, with continued development of the described methods and sampling of adult amphibians and other vertebrates, we expect knowledge of dry body mass in combination with physiological rates and longitudinal models to yield new insights into biogeography, ecogeographical gradients, and evolutionary trade-offs [15,31,101,102]. Finally, this research has applications for understanding the biology of aging, gestation,

obesity, or sleep and how body mass and metabolic rate are related to various disorders and health outcomes in other vertebrates, including humans [25,33,103,104].

Conclusion

Here we presented new models (regression equations) for estimating dry body mass throughout an organism's lifetime using only photographs and morphological measurements. The proposed methods are flexible and provide users with an array of options to suit their particular logistical and analytical needs without harming the *X. laevis* tadpoles. We predict similar future studies will show how morphological measurements will yield accurate estimates of dry body mass in other developmental stages for *X. laevis* and in other vertebrate species. We also proposed many extensions of the developed methods including discussion of obtaining more accurate estimates of dry body mass and using better modelling strategies. Finally, we argue that learning more about dry body mass and density across levels of biological organization and taxonomy has great capacity for advancing our understanding of physiological ecology and even human health.

Tables and Figures

Table 1. Initial input variables used in all models. M is model (see Data analysis in Methods). View is the 3-dimensional origin of each trait. NA is not available, L is lateral, D is dorsal, F is frontal, and Composite is traits obtained from two views. T is tail, Tm is tail muscle, B is body, A is area, L is length, W is width, and H is height. 1 and 2 indicate traits included in the initial and final fits for each model (M1–8), respectively.

View	Units	Trait	Description	M1	M2	M3	M4	M5	M6–8
NA	g	wet mass		1, 2					1, 2
Dorsal	mm	body length	snout-vent		1				1, 2
	mm	body width	postorbital width		1				1, 2
	mm	tail length	vent to end of tail		1				1, 2
	mm	tail width	width at vent		1, 2				1, 2
	mm^2	body area				1			1, 2
	mm^2	tail area				1, 2			1, 2
Lateral	mm	body height	postorbital height		1, 2				1, 2
	mm	tail length			1, 2				1, 2
	mm	tail height	height at vent		1, 2				1, 2
	mm^2	body area				1			1, 2
	mm^2	tail area				1			1, 2
	mm^2	tail muscle area				1			1, 2
	mm^2	fin area	LTA-LTmA			1, 2			1, 2
	mm^2	limb bud area			1, 2	1, 2			1, 2
Frontal	mm	body width	eye to eye		1, 2				1, 2
	mm^2	body area				1, 2			1, 2
Composite	mm^3	body volume 1	LBA*DBW				1		1, 2
	mm^3	body volume 2	LBA*FBW				1		1, 2
	mm^3	body volume 3	LBH*DBA				1, 2		1, 2
	mm^3	body volume 4	DBL*FBA				1		1, 2
	mm^3	tail volume 1	LTA*DTW				1		1, 2
	mm^3	tail volume 2	LTH*DTA				1		1, 2
	mm^3	tail muscle volume	LTmA*DTW				1, 2		1, 2
	mm^3	body volume 5	LBH*DBL*DBW					1, 2	1, 2
	mm^3	tail volume 3	LTH*DTL*DTW					1, 2	1, 2

Table 2. Performance metrics for surveyed models. Rank is the model rank based on MSE and shown only for validation metrics obtained using repeated K-fold cross validation. # Var is the number of final predictor variables. AICc is the Akaike Information Criterion corrected for small sample size for likelihood models. MSE is the mean square error. MAE is the mean absolute error. r^2 is the coefficient of determination. SD is the standard deviation. r^2 is not implemented for Model 7. Model 8 lacks standard deviation estimates because metrics are based on a single testing set of N = 12. The theoretical best model has a high r^2, low errors (MAE or MSE), and a low AICc.

Model (Rank)	# Var	AICc	MSE	MAE	r^2	MSE SD	MAE SD	r^2 SD
1 (8)	1	56.4515	0.1405	0.3050	0.6310	0.0469	0.0566	0.1237
2 (6)	6	38.1121	0.1076	0.2561	0.7192	0.0424	0.0530	0.1182
3 (7)	5	46.4331	0.1181	0.2663	0.6891	0.0494	0.0536	0.1420
4 (2)	2	33.1050	0.0952	0.2392	0.7491	0.0376	0.0491	0.1152
5 (1)	2	30.9366	0.0922	0.2390	0.7546	0.0358	0.0498	0.1110
6 (3)	26	-	0.0996	0.2564	0.7343	0.0331	0.0447	0.1179
7A (4)	6	-	0.1047	0.2568	NA	0.0368	0.0482	NA
7B (5)	5	-	0.1066	0.2603	NA	0.0368	0.0498	NA
8	26	-	0.0563	0.1940	0.7694	NA	NA	NA

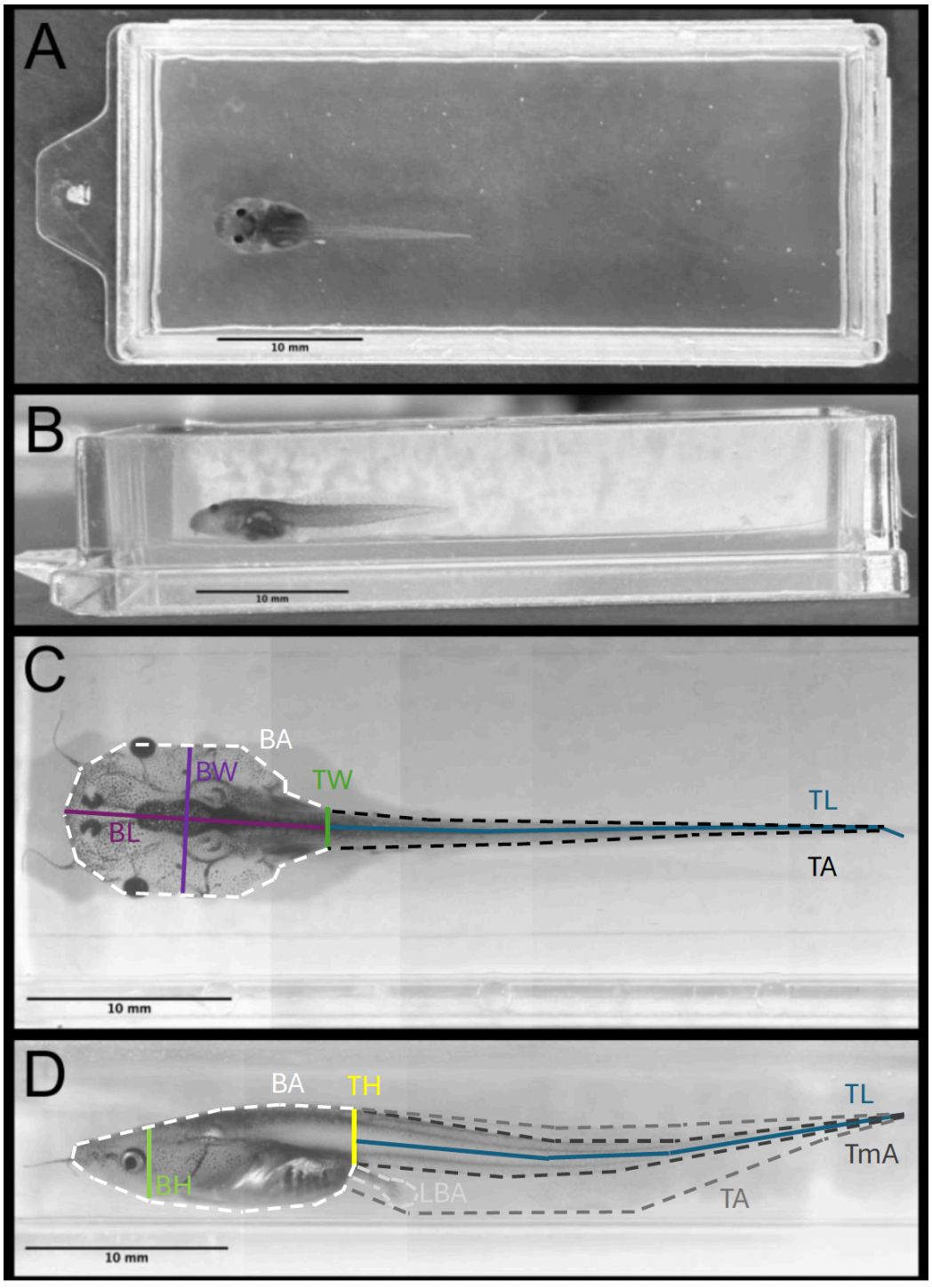

Figure 1. Tadpoles embedded in agarose media and anatomical traits measured. A. Image showing agarose-embedded tadpole in chambered coverglass from dorsal view. B. Image showing agarose-embedded tadpole in chambered coverglass from lateral view. C.Dorsal measurements obtained in this study (see Table 1). D. Lateral measurements obtained in this study (see Table 1). BL is body length, BW is body width, BL is body height, BA is body area, TL is tail length, TW is tail width, TH is tail height, TA is tail area, TmA is tail muscle area, and LBA is limb bud area.

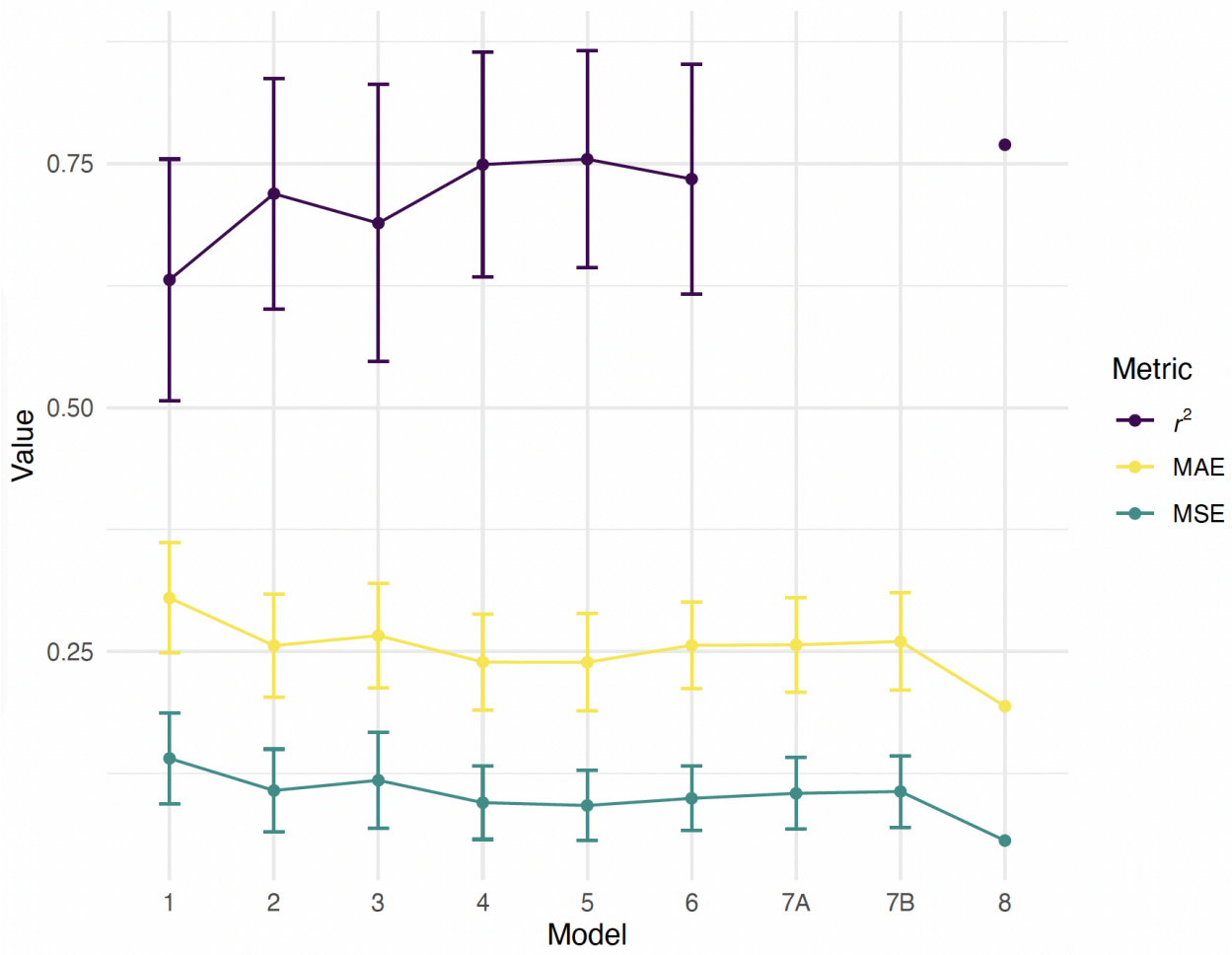

Figure 2. Plot of performance metrics for surveyed models. Models are as in Table 1 and the main text. Models 1–6 are likelihood models and models 6–8 are machine learning models. MAE is the mean absolute error and MSE is the mean square error. Error bars indicate ∓ 1 standard deviation of the mean. r^2 is not implemented for Model 7. Model 8 lacks error bars because metrics are based on a single testing set of N = 12. The theoretical best model has a high r^2 and low errors (MAE or MSE).

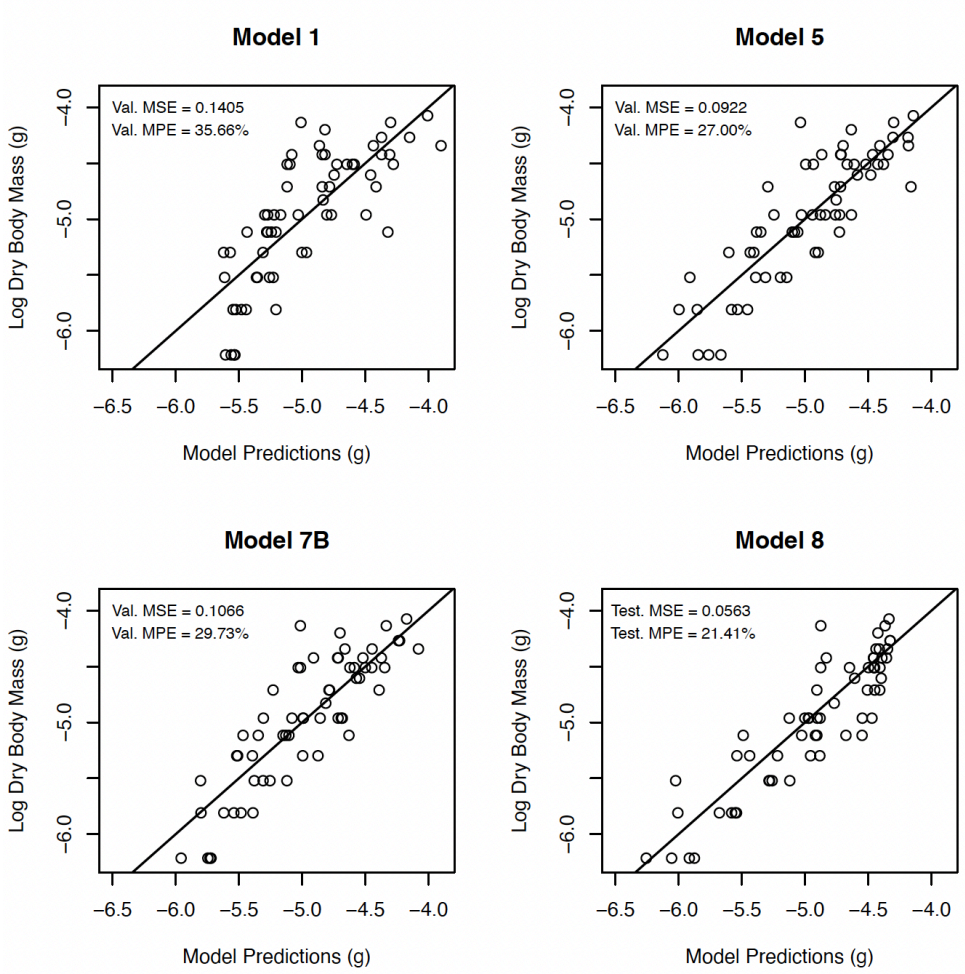

Figure 3. Actual versus predicted plots comparing the wet body mass model (1) to the best likelihood (5), machine learning (7B), and neural network models (8). Each point is an individual tadpole. Val. MSE is the validation mean square error and Val. MPE is the validation mean percentage error. Test. MSE and Test. MPE are the mean square error and mean percentage error for the testing set of Model 8. The solid line is the 1:1 line. The theoretical best model has low errors (MSE, MPE).

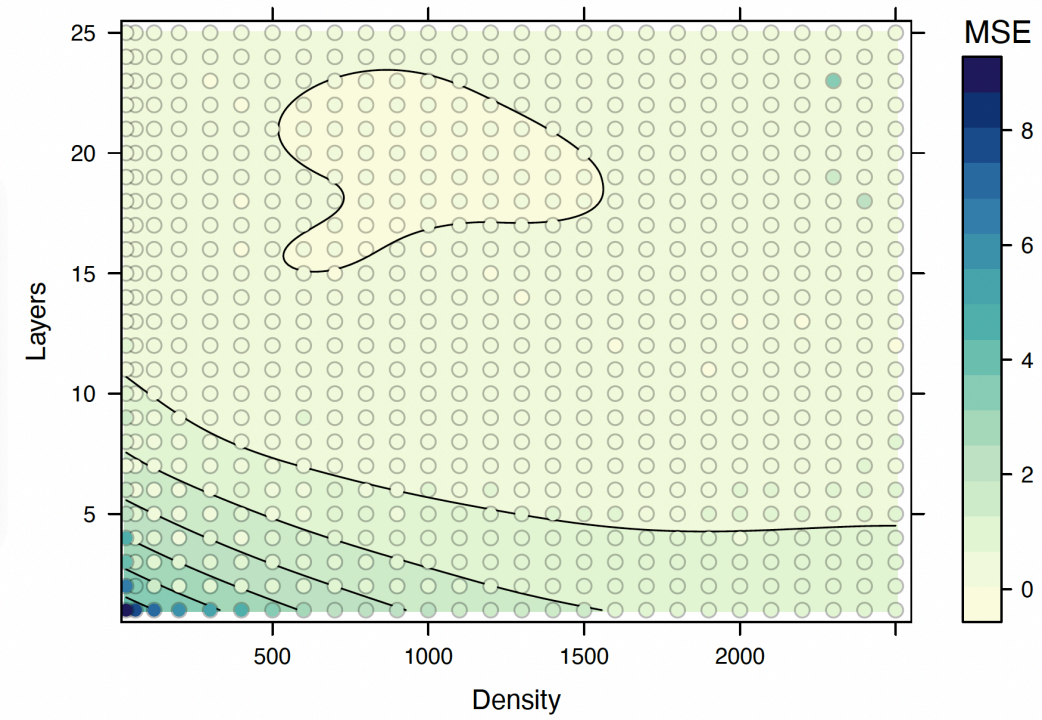

Figure 4. Level plot of hyperparameter search results for neural network (Model 8). Layers is the number of neural layers, density is the number of neurons per layer, and MSE is the (validation) mean square error. Contour lines correspond to the discrete differences in MSE shown in the legend. The network with the lowest validation error had 11 layers and 1900 neurons.

Acknowledgements

We thank the O'Connell lab for valuable feedback regarding the imaging protocol and managing our animal room. We are also indebted to Elizabeth Glynne for her reliability and enthusiasm in showing us how to improve our usage of Fiji.

References

1. Thomson JA. On growth and form. Nature. 1917;100: 21–22.

2. Huxley JS. Relative growth and form transformation. Proc Biol Sci. 1950;137: 465–469.

3. Gayon J. History of the Concept of Allometry. Integr Comp Biol. 2000;40: 748–758.

4. Goldenberg J, Bisschop K, D'Alba L, Shawkey MD. The link between body size, colouration and thermoregulation and their integration into ecogeographical rules: a critical appraisal in light of climate change. Oikos. 2022;2022: e09152.

5. Brown JH, Gillooly JF, Allen AP, Savage VM, West GB. Toward a metabolic theory of ecology. Ecology. 2004;85: 1771–1789.

6. Spotila JR, Berman EN. Determination of skin resistance and the role of the skin in controlling water loss in amphibians and reptiles. Comparative biochemistry and physiology A, Comparative physiology. 1976;55: 407–411.

7. Olson VA, Davies RG, Orme CDL, Thomas GH, Meiri S, Blackburn TM, et al. Global biogeography and ecology of body size in birds. Ecol Lett. 2009;12: 249–259.

8. Woolnough DA, Downing JA, Newton TJ. Fish movement and habitat use depends on water body size and shape. Ecol Freshw Fish. 2009;18: 83–91.

9. Cloyed CS, Grady JM, Savage VM, Uyeda JC, Dell AI. The allometry of locomotion. Ecology. 2021;102: e03369.

10. Gouveia SF, Bovo RP, Rubalcaba JG, Da Silva FR, Maciel NM, Andrade DV, et al. Biophysical modeling of water economy can explain geographic gradient of body size in anurans. Am Nat. 2019;193: 51–58.

11. Rubalcaba JG, Gouveia SF, Olalla-Tárraga MA. A mechanistic model to scale up biophysical processes into geographical size gradients in ectotherms. Glob Ecol Biogeogr. 2019;28: 793–803.

12. Hillebrand H, Azovsky AI. Body size determines the strength of the latitudinal diversity gradient. Ecography (Cop). 2001;24: 251–256.

13. Hone DWE, Benton MJ. The evolution of large size: how does Cope's Rule work? Trends Ecol Evol. 2005;20: 4–6.

14. Galván I, Schwartz TS, Garland T Jr. Evolutionary physiology at 30+: Has the promise been fulfilled?: Advances in Evolutionary Physiology: Advances in Evolutionary Physiology. Bioessays. 2022;44: e2100167.

15. White CR, Alton LA, Bywater CL, Lombardi EJ, Marshall DJ. Metabolic scaling is the product of life-history optimization. Science. 2022;377: 834–839.

16. Glazier DS. A unifying explanation for diverse metabolic scaling in animals and plants. Biol Rev Camb Philos Soc. 2010;85: 111–138.

17. Albright TP, Mutiibwa D, Gerson AR, Smith EK, Talbot WA, O'Neill JJ, et al. Mapping evaporative water loss in desert passerines reveals an expanding threat of lethal dehydration. Proc Natl Acad Sci U S A. 2017;114: 2283–2288.

18. Hessen DO, Elser JJ, Sterner RW, Urabe J. Ecological stoichiometry: An elementary approach using basic principles. Limnol Oceanogr. 2013;58: 2219–2236.

19. Makarieva AM, Gorshkov VG, Li B-L, Chown SL, Reich PB, Gavrilov VM. Mean mass-specific metabolic rates are strikingly similar across life's major domains: Evidence for life's metabolic optimum. Proc Natl Acad Sci U S A. 2008;105: 16994–16999.

20. Haemmerich D, dos Santos I, Schutt DJ, Webster JG, Mahvi DM. In vitro measurements of temperature-dependent specific heat of liver tissue. Med Eng Phys. 2006;28: 194–197.

21. Suarez RK. Hummingbird flight: sustaining the highest mass-specific metabolic rates among vertebrates. Experientia. 1992;48: 565–570.

22. Robinson WR, Peters RH, Zimmermann J. The effects of body size and temperature on metabolic rate of organisms. Can J Zool. 1983;61: 281–288.

23. Daan S, Masman D, Groenewold A. Avian basal metabolic rates: their association with body composition and energy expenditure in nature. Am J Physiol. 1990;259: R333–40.

24. Zhang R, Zhao T, Lu Y, Xu X. Relaxed adaptive lasso and its asymptotic results. Symmetry (Basel). 2022;14: 1422.

25. Bell AW, Battaglia FC, Makowski EL, Meschia G. Relationship between metabolic rate and body size in fetal life. Biol Neonate. 1985;47: 120–123.

26. Van Voorhies WA, Khazaeli AA, Curtsinger JW. Lack of correlation between body mass and metabolic rate in Drosophila melanogaster. J Insect Physiol. 2004;50: 445–453.

27. Bell AW, Battaglia FC, Meschia G. Relation between metabolic rate and body size in the ovine fetus. J Nutr. 1987;117: 1181–1186.

28. Nagy KA. Field metabolic rate and food requirement scaling in mammals and birds. Ecol Monogr. 1987;57: 111–128.

29. Zheng W-H, Liu J-S, Swanson DL. Seasonal phenotypic flexibility of body mass, organ masses, and tissue oxidative capacity and their relationship to resting metabolic rate in Chinese bulbuls. Physiol Biochem Zool. 2014;87: 432–444.

30. Ikeda T. Metabolic rates of epipelagic marine zooplankton as a function of body mass and temperature. Mar Biol. 1985;85: 1–11.

31. Konarzewski M, Diamond J. Evolution of basal metabolic rate and organ masses in laboratory mice. Evolution. 1995;49: 1239–1248.

32. Sparti A, DeLany JP, de la Bretonne JA, Sander GE, Bray GA. Relationship between resting metabolic rate and the composition of the fat-free mass. Metabolism. 1997;46: 1225–1230.

33. Zhang K, Sun M, Werner P, Kovera AJ, Albu J, Pi-Sunyer FX, et al. Sleeping metabolic rate in relation to body mass index and body composition. Int J Obes Relat Metab Disord. 2002;26: 376–383.

34. Glazier DS. Body-mass scaling of metabolic rate: What are the relative roles of cellular versus systemic effects? Biology (Basel). 2015;4: 187–199.

35. Bennett BD, Yuan J, Kimball EH, Rabinowitz JD. Absolute quantitation of intracellular metabolite concentrations by an isotope ratio-based approach. Nat Protoc. 2008;3: 1299–1311.

36. Juarez BH, Quintanilla-Salinas I, Lacey MP, O'Connell LA. Water availability and temperature as modifiers of evaporative water loss in tropical frogs. Integr Comp Biol. 2024;64: 354–365.

37. McLean JA, Speakman JR. Effects of body mass and reproduction on the basal metabolic rate of brown long-eared bats (Plecotus auritus). Physiol Biochem Zool. 2000;73: 112–121.

38. Niitepõld K, Boggs CL. Effects of increased flight on the energetics and life history of the butterfly Speyeria mormonia. PLoS One. 2015;10: e0140104.

39. Ricklefs R, Konarzewski M, Daan S. The relationship between basal metabolic rate and daily energy expenditure in birds and mammals. Am Nat. 1996;147: 1047–1071.

40. Meerlo P, Bolle L, Visser GH, Masman D, Daan S. Basal metabolic rate in relation to body composition and daily energy expenditure in the field vole, Microtus agrestis. Physiol Zool. 1997;70: 362–369.

41. Glazier DS. Is metabolic rate a universal "pacemaker" for biological processes? Biol Rev Camb Philos Soc. 2015;90: 377–407.

42. Roderick ML. On the measurement of growth with applications to the modelling and

analysis of plant growth: Measuring growth. Funct Ecol. 2000;14: 244–251.

43. Sosik HM, Olson RJ, Neubert MG, Shalapyonok A, Solow AR. Growth rates of coastal phytoplankton from time-series measurements with a submersible flow cytometer. Limnol Oceanogr. 2003;48: 1756–1765.

44. Boye E, Løbner-Olesen A. Bacterial growth control studied by flow cytometry. Res Microbiol. 1991;142: 131–135.

45. Huxley JS. Problems of relative growth Methuen. London, UK. 1932.

46. Goldman CA, Snell RR, Thomason JJ, Brown DB. Principles of allometry. Tested studies for laboratory teaching. 1990;11: 43–72.

47. Davies HG, Deeley EM. An integrator for measuring the dry mass of cells and isolated components. Exp Cell Res. 1956;11: 169–185.

48. Bergstedt A, Olesen PO. Models for Predicting Dry Matter Content of Norway spruce. Scand J For Res. 2000;15: 633–644.

49. Baumgärtner D, Rothhaupt K-O. Predictive length–dry mass regressions for freshwater invertebrates in a pre-Alpine Lake littoral. Int Rev Hydrobiol. 2003;88: 453–463.

50. Johnston TA, Cunjak RA. Dry mass–length relationships for benthic insects: a review with new data from Catamaran Brook, New Brunswick, Canada: Mass-length relationships in benthic studies. Freshw Biol. 1999;41: 653–674.

51. Martins R, Melo AS, Gonçalves J, Hamada N. Estimation of dry mass of caddisflies Phylloicus elektoros (Trichoptera: Calamoceratidae) in a Central Amazon stream. Zoologia (Curitiba). 2014;31: 337–342.

52. Cressa C. Dry mass estimation of tropical aquatic insects using different short-term preservation methods. Rev Biol Trop. 1999;47: 143–149.

53. Moen DS, Irschick DJ, Wiens JJ. Evolutionary conservatism and convergence both lead to striking similarity in ecology, morphology and performance across continents in frogs. Proc Biol Sci. 2013;280: 20132156.

54. Vervust B, Van Dongen S, Van Damme R. The effect of preservation on lizard morphometrics – an experimental study. Amphib-reptil. 2009;30: 321–329.

55. Shu G, Gong Y, Xie F, Wu NC, Li C. Effects of long-term preservation on amphibian body conditions: implications for historical morphological research. PeerJ. 2017;5: e3805.

56. Sotola VA, Craig CA, Pfaff PJ, Maikoetter JD, Martin NH, Bonner TH. Effect of preservation on fish morphology over time: Implications for morphological studies.

PLoS One. 2019;14: e0213915.

57. Baken EK, Mellenthin LE, Adams DC. Macroevolution of desiccation-related morphology in plethodontid salamanders as inferred from a novel surface area to volume ratio estimation approach. Evolution. 2020;74: 476–486.

58. Juarez BH, Adams DC. Evolutionary allometry of sexual dimorphism of jumping performance in anurans. Evol Ecol. 2021. doi:10.1007/s10682-021-10132-x

59. Juarez BH, Moen DS, Adams DC. A Morphological Method to Approximate Jumping Performance in Anurans for Macroevolutionary Studies. Evol Biol. 2020;47: 260–271.

60. Green SL. The Laboratory Xenopus Sp. London, England: CRC Press; 2009. Available: https://books.google.com/books?hl=en&lr=&id=5WTMBQAAQBAJ&oi=fnd&pg=PP1&dq=xenopus+review+medical+suppliers&ots=yGxfCaltsc&sig=S1aW-FZCuueXMkLq0Ve48qGCJZM

61. Ishibashi S, Saldanha FYL, Amaya E. Xenopus as a model organism for biomedical research. In: Jalali M, Saldanha FYL, Jalali M, editors. Basic Science Methods for Clinical Researchers. Elsevier; 2017. pp. 263–290.

62. Snodgrass JW, Hopkins WA, Roe JH. Relationships among developmental stage, metamorphic timing, and concentrations of elements in bullfrogs (Rana catesbeiana). Environ Toxicol Chem. 2003;22: 1597–1604.

63. Gerlach J, Gerlach R. Reproduction in the tree frog Tachycnemis seychellensis. 2010. Available: https://www.researchgate.net/profile/Justin-Gerlach/publication/266295930_Reproduction_in_the_tree_frog_Tachycnemis_seychellensis/links/54b5121c0cf26833efd061b7/Reproduction-in-the-tree-frog-Tachycnemis-seychellensis.pdf

64. Duellman WE, Trueb L. Biology of amphibians. JHU Press; 1994.

65. Fan XL, Lin ZH, Scheffers BR. Physiological, developmental, and behavioral plasticity in response to thermal acclimation. J Therm Biol. 2021;97: 102866.

66. Kruger N, Secondi J, du Preez L, Herrel A, Measey J. Phenotypic variation in Xenopus laevis tadpoles from contrasting climatic regimes is the result of adaptation and plasticity. Oecologia. 2022;200: 37–50.

67. Schlippe Justicia L, Fouilloux CA, Rojas B. Poison frog social behaviour under global change: potential impacts and future challenges. Acta Ethol. 2023;26: 151–166.

68. Vargas-Salinas F, Rojas B. Developments in the study of poison frog evolutionary ecology I: social interactions, life history and habitat use across space and

ontogeny. Evol Ecol. 2024;38: 1–22.

69. Blackiston DJ, Levin M. Ectopic eyes outside the head in Xenopus tadpoles provide sensory data for light-mediated learning. J Exp Biol. 2013;216: 1031–1040.

70. Granados Frias D, Akbari N, A O'Connell L, Juarez B. Non-lethal 3-D imaging techniques for estimating tadpole morphology v1. protocols.io; 2025 Jan. doi:10.17504/protocols.io.rm7vzk1wrvx1/v1

71. Schindelin J, Arganda-Carreras I, Frise E, Kaynig V, Longair M, Pietzsch T, et al. Fiji: an open-source platform for biological-image analysis. Nat Methods. 2012;9: 676–682.

72. Zou H. The adaptive lasso and its oracle properties. J Am Stat Assoc. 2006;101: 1418–1429.

73. Thompson CG, Kim RS, Aloe AM, Becker BJ. Extracting the variance inflation factor and other multicollinearity diagnostics from typical regression results. Basic Appl Soc Psych. 2017;39: 81–90.

74. Kuhn M. Building Predictive Models in R Using the caret Package. J Stat Softw. 2008;28: 1–26.

75. R Core Team. R: A Language and Environment for Statistical Computing. R Foundation for Statistical Computing, Vienna, Austria; 2024. Available: https://www.R-project.org/

76. Friedman J, Hastie T, Tibshirani R. Regularization paths for generalized linear models via coordinate descent. J Stat Softw. 2010;33: 1–22.

77. Tay JK, Narasimhan B, Hastie T. Elastic net regularization paths for all generalized linear models. J Stat Softw. 2023;106: 1–31.

78. Allaire J, Tang Y. tensorflow: R Interface to "TensorFlow." 2024. Available: https://CRAN.R-project.org/package=tensorflow

79. Kalinowski T, Allaire J, Chollet F. keras3: R Interface to "Keras." 2024. Available: https://CRAN.R-project.org/package=keras3

80. Heaton J. Introduction to Neural Networks for Java. Heaton Research. 2008. Available: https://books.google.com/books?hl=en&lr=&id=Swlcw7M4uD8C&oi=fnd&pg=PR21&dq=Introduction+to+Neural+Networks+with+Java&ots=TMw7P9e_v0&sig=NUaEmARsI4NZF-BV6LJZa7Jc8aQ

81. Uzair M, Jamil N. Effects of Hidden Layers on the Efficiency of Neural networks. 2020 IEEE 23rd International Multitopic Conference (INMIC). IEEE; 2020. pp. 1–6.

82. Wanas N, Auda G, Kamel MS, Karray F. On the optimal number of hidden nodes in a neural network. Conference Proceedings IEEE Canadian Conference on Electrical and Computer Engineering (Cat No98TH8341). IEEE; 2002. pp. 918–921 vol.2.

83. Zeiler MD, Ranzato M, Monga R, Mao M, Yang K, Le QV, et al. On rectified linear units for speech processing. 2013 IEEE International Conference on Acoustics, Speech and Signal Processing. IEEE; 2013. pp. 3517–3521.

84. Kingma DP, Ba J. Adam: A method for stochastic optimization. arXiv [cs.LG]. 2014. Available: http://arxiv.org/abs/1412.6980

85. Zeng X, Martinez TR. Distribution-balanced stratified cross-validation for accuracy estimation. J Exp Theor Artif Intell. 2000;12: 1–12.

86. Schenk T, Quarter A. Introduction to Photogrammetry. The Ohio State University, Columbus. 2005. Available: https://www.academia.edu/download/58585147/IntroPhoto.pdf

87. Beltran RS, Ruscher-Hill B, Kirkham AL, Burns JM. An evaluation of three-dimensional photogrammetric and morphometric techniques for estimating volume and mass in Weddell seals Leptonychotes weddellii. PLoS One. 2018;13: e0189865.

88. Van Den Noortgate W, Onghena P. Parametric and nonparametric bootstrap methods for meta-analysis. Behav Res Methods. 2005;37: 11–22.

89. Lee SMS, Young GA. Parametric bootstrapping with nuisance parameters. Stat Probab Lett. 2005;71: 143–153.

90. Adams R, Cain Z, Assis R, DeGiorgio M. Robust phylogenetic regression. Syst Biol. 2024. Available: https://academic.oup.com/sysbio/article-abstract/73/1/140/7456117

91. Cantoni E, Ronchetti E. Robust inference for generalized linear models. J Am Stat Assoc. 2001;96: 1022–1030.

92. Collyer ML, Adams DC. Interrogating random and systematic measurement error in morphometric data. Evol Biol. 2024;51: 179–207.

93. Fuller WA. Measurement Error Models. 99th ed. Nashville, TN: John Wiley & Sons; 2009.

94. Baxter D, Cohen KE, Donatelli CM, Tytell ED. Internal vertebral morphology of bony fishes matches the mechanical demands of different environments. Ecol Evol. 2022;12: e9499.

95. Iijima M, Kubo T. Vertebrae-based body length estimation in crocodylians and its

implication for sexual maturity and the maximum sizes. Integr Org Biol. 2020;2: obaa042.

96. Iijima M, Kubo T. Comparative morphology of presacral vertebrae in extant crocodylians: taxonomic, functional and ecological implications. Zool J Linn Soc. 2019;186: 1006–1025.

97. Glazier DS. Effects of Contingency versus Constraints on the Body-Mass Scaling of Metabolic Rate. Challenges. 2018;9: 4.

98. Glazier DS. Activity alters how temperature influences intraspecific metabolic scaling: testing the metabolic-level boundaries hypothesis. J Comp Physiol B. 2020;190: 445–454.

99. Glazier DS. Activity affects intraspecific body-size scaling of metabolic rate in ectothermic animals. J Comp Physiol B. 2009;179: 821–828.

100. Adams DC, Collyer ML. Extending phylogenetic regression models for comparing within‐species patterns across the tree of life. Methods Ecol Evol. 2024;15: 2234–2246.

101. Shokri M, Cozzoli F, Vignes F, Bertoli M, Pizzul E, Basset A. Metabolic rate and climate change across latitudes: evidence of mass-dependent responses in aquatic amphipods. J Exp Biol. 2022;225: jeb244842.

102. Marquet P, Labra FA, Maurer BA. Metabolic Ecology: Linking individuals to ecosystems. Ecology. 2004;85: 1794–1796.

103. Greenberg JA, Boozer CN. Metabolic mass, metabolic rate, caloric restriction, and aging in male Fischer 344 rats. Mech Ageing Dev. 2000;113: 37–48.

104. Luke A, Schoeller DA. Basal metabolic rate, fat-free mass, and body cell mass during energy restriction. Metabolism. 1992;41: 450–456.